Measurement of Charged-Particle Stopping in Warm Dense Plasma

A. B. Zylstra,[1,*] J. A. Frenje,[1] P. E. Grabowski,[2] C. K. Li,[1] G. W. Collins,[3] P. Fitzsimmons,[4] S. Glenzer,[5] F. Graziani,[3] S. B. Hansen,[6] S. X. Hu,[7] M. Gatu Johnson,[1] P. Keiter,[8] H. Reynolds,[4] J. R. Rygg,[3] F. H. Séguin,[1] and R. D. Petrasso[1]

[1]*Plasma Science and Fusion Center, Massachusetts Institute of Technology, Cambridge, Massachusetts 02139, USA*
[2]*University of California Irvine, Irvine, California 92697, USA*
[3]*Lawrence Livermore National Laboratory, Livermore, California 94550, USA*
[4]*General Atomics, San Diego, California 92186, USA*
[5]*SLAC National Accelerator Laboratory, Menlo Park, California 94025, USA*
[6]*Sandia National Laboratories, Albuquerque, New Mexico 87185, USA*
[7]*Laboratory for Laser Energetics, University of Rochester, Rochester, New York 14623, USA*
[8]*University of Michigan, Ann Arbor, Michigan 48109, USA*

(Received 8 February 2015; published 27 May 2015)

We measured the stopping of energetic protons in an isochorically heated solid-density Be plasma with an electron temperature of ~32 eV, corresponding to moderately coupled $[(e^2/a)/(k_B T_e + E_F) \sim 0.3]$ and moderately degenerate $[k_B T_e/E_F \sim 2]$ "warm-dense matter" (WDM) conditions. We present the first high-accuracy measurements of charged-particle energy loss through dense plasma, which shows an increased loss relative to cold matter, consistent with a reduced mean ionization potential. The data agree with stopping models based on an *ad hoc* treatment of free and bound electrons, as well as the average-atom local-density approximation; this work is the first test of these theories in WDM plasma.

DOI: 10.1103/PhysRevLett.114.215002 PACS numbers: 52.25.Tx, 52.20.Hv, 71.10.Ca

Studying charged-particle stopping in dense plasmas is relevant to fundamental plasma physics and to the potential realization of laboratory-scale thermonuclear fusion. Dense plasmas in the warm-dense matter (WDM) regime, approximately solid density and tens of eV temperature, are of great interest as a probe of stopping-power theories, with broader physics relevance to nonequilibrium statistical mechanics [1], dense plasma transport properties [2–4], and bound-free transitions in WDM plasmas [5]. Accurate theory for bound-free transitions is required to interpret data obtained with common laser-plasma diagnostics including Thomson scattering [6] and opacity-based areal density techniques [7].

In inertial confinement fusion (ICF), spherical implosion heats and compresses a small volume of fuel to, in principle, spark a runaway thermonuclear burn wave [8–10]. This burn wave propagates via fusion-produced energetic α particle self-heating. Understanding the transport of these α's in plasmas at extreme conditions is required to accurately model ignition experiments at the National Ignition Facility (NIF) [11], where significant α self-heating has recently been achieved [12]. Charged-particle transport in and heating of dense plasmas is also highly relevant to alternative particle-beam-driven inertial fusion designs such as heavy-ion fusion [13] and proton fast ignition [14,15].

The stopping of energetic charged particles has been studied in cold (room-temperature) material for a century [16]; there, the energetic particle loses energy to bound electrons, for which theoretical models [17,18] are fit to a significant experimental database [19]. In a plasma, an energetic particle simultaneously interacts with a large number of particles via the Coulomb force, over a volume with dimensions given by the screening length (Debye-Hückel or Thomas-Fermi). Typically the stopping is treated as either a summation of two-body (binary) collisions [20–22], or a dielectric (density) response [22–25].

In this Letter, we report the first high-precision measurement of charged-particle energy loss in a dense moderately degenerate and moderately coupled plasma. The results are compared to theories in common use by simulation codes. For testing theory in this regime, these results are a significant improvement on previous experiments, which utilized simpler low-density non-degenerate plasmas [26–31] or had significantly less precision [32].

The OMEGA laser facility [33] was used to create a pulsed monoenergetic source of protons that probe a subject plasma isochorically heated to WDM conditions. Figure 1 shows the experimental configuration. A shock-driven "exploding pusher" implosion [34] filled with D^3He fuel is used to produce the probing protons via the fusion reaction

$$D + {}^3He \rightarrow {}^4He + p(14.63\ \text{MeV}). \quad (1)$$

The implosion is driven by 20 of the OMEGA laser beams at 3ω (351 nm), delivering 10 kJ of energy in a 1 ns duration square pulse. These protons, produced over a ~100 *ps* burst, then traverse the x-ray isochorically heated subject plasma. The subject target consists of a plastic (CH) tube coated with 1–2 μm of Ag, with an inner diameter of

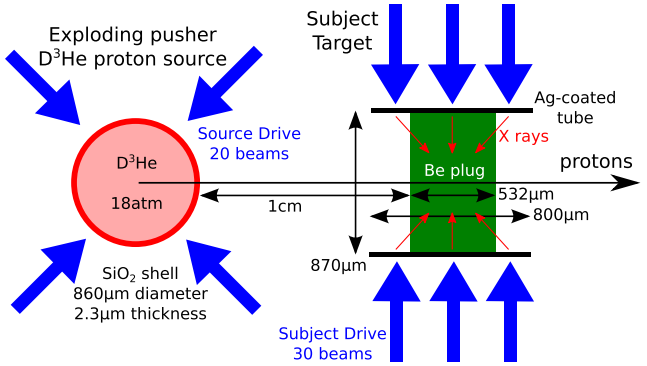

FIG. 1 (color online). Experimental geometry. A thin-glass exploding-pusher proton source (left) imploded by 20 laser beams creates energetic D^3He protons used to probe a subject plasma, which is created by isochorically heating a solid Be plug with x rays (right). These x rays are created by the 30 laser beams irradiating the Ag-coated CH tube.

870 μm, a wall thickness of 24 μm, and 800 μm in length. A cylindrical Be plug is inserted into the tube, with total $\rho L = 94.2 \pm 0.6$ mg/cm^2, which serves as the subject material for the experiment [35]. Thirty of the OMEGA beams are incident upon the outer surface of the tube, arranged in three rings positioned along the axis of the cylinder. The lasers are defocused to create ~100 μm diameter illumination spots on the cylinder. The total drive energy on the subject target was 15 kJ, delivered in a 1 ns square pulse. The resulting intensity in each spot is ~10^{15} W/cm^2. This laser intensity generates Ag L-shell emission at 3–4 keV in the corona surrounding the cylindrical target, which volumetrically heats the Be plug as the attenuation length in solid Be is 300–500 μm, comparable to the cylinder's dimensions. The heating occurs over 1 ns, and the temperature is quiescent for another ns after the drive turns off [36]. The implosion proton source was timed so that the proton probing occurs at 1.4 ns after the onset of the heating beams, at which time electrostatic charging [29,37] of the subject target is negligible [38].

The x-ray isochoric-heating technique used in this work has been used extensively at OMEGA for dense plasma physics studies [36,39–41]. The subject target used here mimics the previous experiments [42]. This technique is uniquely appropriate for stopping-power measurements. Relative to other techniques such as shock compression and proton isochoric heating, the x-ray isochoric heating technique is advantageous in that it produces a large, quiescent, and homogenous plasma.

The isochoric and homogenous nature of the heated plasma comes from several effects. First, the sound speed in solid-density Be is $c_s = \sqrt{\gamma \bar{Z} k_B T_e / m_i} \approx 4 \times \sqrt{\bar{Z} T_e}\,\mu$m/ns, where T_e is the electron temperature in eV, $\bar{Z}$ is the ionization state, and γ is the adiabatic index. The sound speed for these conditions is of order tens of μm/ns; since scale lengths are hundreds of μm and time scales are of order of ns, significant hydrodynamic motion of the Be cannot occur. Second, the laser interaction on the outside of the cylinder does not interact hydrodynamically with the Be sample, since the inward-propagating shock wave does not reach the inner material region probed by the protons at the sampling time. This was verified with radiation-hydrodynamics simulations.

Since the mass density is constant, the heated plasma conditions are characterized by the electron temperature (T_e) and the ionization state of the Be ($\bar{Z}$). These are inferred from very similar experiments (Fig. 9 of Ref. [36]). The electron temperature, which defines the ionization state (or free-electron density), is set by the x-ray heating. As the drive energy was the same as in previous experiments (15 kJ/1 ns), we assumed that the conversion of laser energy to L-shell emission is comparable in these experiments, corrected for attenuation in the plastic tube used (12%) and a larger volume of Be (45%). Using this information, the temperature is estimated to be $T_e = 32$ eV. The T_e data in previous experiments had an uncertainty of ± 5.5 eV; in the following analysis, this is increased to ± 15 eV to include any uncertainty in the scaling. The ionization state using the Glenzer data is then $\bar{Z} = 2.46 \pm 0.15$, corresponding to a free-electron density of $n_e = (2.91 \pm 0.18) \times 10^{23}$ 1/cm^3. Alternatively, using $T_e = 32 \pm 15$ eV and the Muze local density approximation (LDA) model gives $\bar{Z} = 2.28^{+0.42}_{-0.27}$, consistent with the data.

This plasma can be understood by the dimensionless parameters for degeneracy (θ) and coupling (Γ_e),

$$\theta \equiv \frac{k_B T_e}{E_F}, \qquad \Gamma_e \equiv \frac{e^2}{a(k_B T_e + E_F)}, \tag{2}$$

where θ is the ratio of the thermal to Fermi energy (E_F), and Γ_e is the ratio of the electron interparticle Coulomb potential energy to average kinetic energy ($k_B T_e + E_F$), where $a = [3/(4\pi n_e)]^{1/3}$ is the Wigner-Seitz radius. At these conditions, $\theta \approx 2$ and $\Gamma_e \approx 0.3$, indicating moderate degeneracy and coupling. The parameter space for the degeneracy and coupling versus electron density and temperature is shown in Fig. 2, with this work and prior experiments marked. We note that the Graziani *et al.* (Ref. [32]) experiments are close to this work in parameter space, but the uncertainty in their stopping-power data is significantly larger, and they were unable to differentiate any stopping models. In Ref. [32], the stopping-power uncertainty reported was ~24%. In this work, the use of monoenergetic D^3He protons, wedge range filter (WRF) proton spectrometers [43,44] with intrinsic energy uncertainty ~40 keV [45], and a large subject plasma with $\rho L \sim 100$ mg/cm^2 enable stopping-power measurements with precision of ~1.5%. On each shot, several WRFs were used: three WRFs measured the spectrum emitted from the source, while one measured the downshifted protons

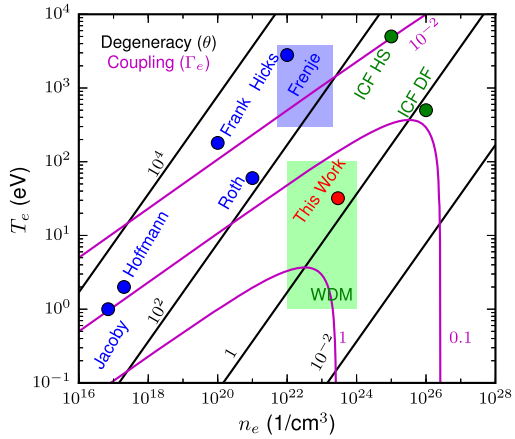

FIG. 2 (color online). Parameter space, showing contours of constant degeneracy (θ, black) and coupling (Γ_e, magenta) as functions of electron density and temperature. Previous experiments [26–31] are shown by blue points (blue shaded region for Ref. [31]), and this work is shown by the red points. A typical range for WDM ($n_e = 10^{22}$–10^{24} 1/cm^3, T_e = 1–100 eV) is shown by the green shaded box, while typical parameters for the ICF hot spot (HS) and dense fuel (DF) are shown by green points.

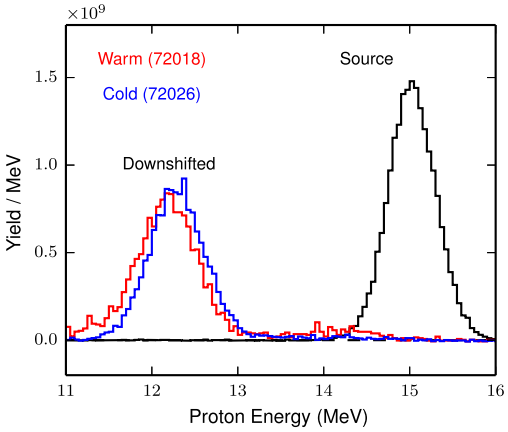

FIG. 3 (color online). Proton spectral data for a heated (warm) Be target (shot 72018, red) and an undriven (cold) Be target (shot 72026, blue). For each shot, the proton source spectrum (black) is measured directly by three detectors.

traversing the Be plasma. For the protons traversing the Be plasma, the small WRF solid angle corresponds to measuring protons traversing a ~400 μm diameter cross section in the center of the Be plasma.

Shots were taken with both undriven (i.e., cold) and heated (warm) Be targets. Data from each type of shot are shown in Fig. 3. Three WRFs measured the source spectrum; each is fit with a Gaussian to determine the mean energy. The weighted mean of the three measurements represents the initial proton energy, where the primary source of uncertainty is the WRF response and only relative (random or statistical) uncertainties are retained. Systematic calibration uncertainty is correlated between the WRFs since they are calibrated against the same proton source [46]. The D^{3}He proton spectra are Doppler-broadened due to the plasma temperature and upshifted slightly from their birth energy [Eq. (1)] due to radial electric fields around the exploding-pusher implosion [29]. The initial (E_i) and final (E_f) proton energies are determined from a Gaussian fit; the downshift, or total energy loss, is $\Delta E \equiv E_i - E_f$. The measured quantities for each shot are given in Table I. The data clearly show a larger ΔE in the plasma case than in the cold (undriven) case, which means that the stopping power increases in the WDM plasma.

For comparison, the energy loss can be obtained from theory by integrating the stopping power over the path-length traversed [47],

$$\Delta E = -\int_0^L \frac{dE}{dx}\,dx, \tag{3}$$

where dE/dx depends on the particle energy and plasma conditions. A comparison of our data to several theories is shown in Fig. 4. The measurement uncertainty is due to the proton spectroscopy uncertainties. In the cold-matter theory calculations the primary uncertainty is the areal density uncertainty and initial energy variations, while the plasma theory uncertainties are dominated by the uncertainty in plasma conditions (n_e, T_e, and $\bar{Z}$ where applicable).

First, we compare our cold data to the well-established SRIM [19] and ICRU [48] stopping powers, derived from fits to prior data, which show good agreement given our measurement uncertainty and an expected ~1% uncertainty in the SRIM/ICRU databases (not included in Fig. 4 error bars).

The warm data (shots 72018 and 72024) show a clear enhancement in stopping power (downshift) relative to the cold material. dE/dx is enhanced by the long-range nature of stopping on the plasma (free) electrons relative to the atomic (bound) electrons. There are three common theoretical techniques for treating the partially ionized material in the warm subject plasma: either an *ad hoc* combination of independent bound- and free-electron components [49,50], or using an inhomogeneous WDM theory such as the average-atom local-density approximation (AA-LDA) model [51,52], or with a Bethe-style effective ionization potential.

In the first case, the partially ionized plasma is approximated by treating free and bound electrons entirely separately; we use Zimmerman's model [50] for the bound

TABLE I. Data summary: initial (E_i) and final (E_f) energies, and downshift (ΔE) for each shot.

Shot	E_i (MeV)	E_f (MeV)	ΔE (MeV)
72018 (Warm)	15.019 ± 0.020	12.167 ± 0.039	2.851 ± 0.044
72024 (Warm)	15.025 ± 0.029	12.043 ± 0.037	2.981 ± 0.047
72025 (Cold)	15.075 ± 0.018	12.355 ± 0.036	2.720 ± 0.040
72026 (Cold)	15.004 ± 0.017	12.296 ± 0.040	2.708 ± 0.044

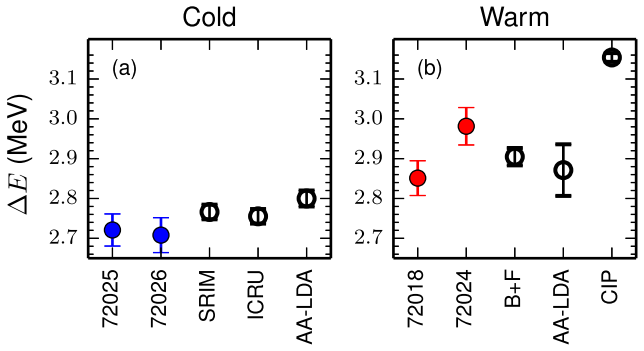

FIG. 4 (color online). Downshift (ΔE) for cold (a) and warm (b) shots compared to theory. The solid points are data (denoted by shot number), and theories are hollow points. The uncertainties in theoretical calculations are due to uncertainties in ρL and plasma conditions.

electrons, where a Bethe-Bloch style Coulomb logarithm term is used with a mean ionization potential. For the free electrons, any plasma stopping model which properly reduces to the quantum RPA limit at high particle velocity can be used, such as the Maynard-Deutsch [25] or Brown-Preston-Singleton [53] which give nearly identical results. This *ad hoc* bound + free model is shown in Fig. 4 as "$B + F$." In this regime, the approximation agrees with the experimental results. The uncertainty in the theoretical value results from the experimental uncertainties in T_e and $\bar{Z}$.

Second, the partially ionized material can be treated with the AA-LDA model [54], which allows for a self-consistent first-principles treatment of the inhomogeneous electron distribution around an ion ("local"). The inhomogeneities in the electron distribution are, in essence, the system's partial ionization. The AA-LDA stopping-power result is shown in Fig. 4, also showing agreement with the experimental data. The uncertainty in the calculated downshift results from the experimental uncertainty in T_e.

Finally, we compare to a "classical ideal plasma" (CIP) in Fig. 4b, which is calculated using a nondegenerate BPS stopping power with an assumed fully-ionized homogenous plasma, i.e., neglecting the partial ionization of this system. This model clearly disagrees with the data, demonstrating the importance of the partial ionization for stopping in this regime.

In calculating the total stopping power, the electron temperature and degeneracy have little direct effect ($\ll 1\%$). This is because the D^3He proton velocity is very high relative to the plasma electron thermal velocity, so this experiment is in the high-energy Bethe stopping limit. However, the heating affects the ionization state and thus the stopping power. The data thus serve as a sensitive probe of the relative importance of bound-free and free-free collisions in each case (cold vs warm), as the electron "configuration" causes the increased stopping in the WDM plasma through an increase in the average energy transferred to a plasma electron during a collision. This can be modeled using a Bethe-style stopping-power equation,

$$\frac{dE}{dx} = -\frac{4\pi Z_t^2 e^4}{m_e v_t^2} n_e \ln\left[\frac{2m_e v_t^2}{\bar{I}}\right], \tag{4}$$

where physically, in the Coulomb logarithm, $2m_e v_t^2$ represents the maximum energy transfer to an electron (a head-on collision), and $\bar{I}$ is the "mean ionization potential" representing the minimum energy transfer, which is sensitive to the electron configuration (bound vs free). This is a simple form of the Coulomb logarithm, neglecting quantum diffraction, dynamical screening, and strong collisions [55,56], but this form can be used to further understand the experimental data. We fit the downshift data using the known target areal density and Eq. (4) to infer $\bar{I}$. The best-fit values are shown in Fig. 5. The data clearly show a higher $\bar{I}$ in the cold case than in the warm, which corresponds to the observed increase in stopping power (Fig. 4). The inferred values of $\bar{I}$ show good agreement with the Andersen-Ziegler value [57] in the cold-matter stopping case. The ideal high-energy-projectile plasma limit, $\bar{I} = \hbar\omega_{pe}$, represents a lower bound on $\bar{I}$, shown by the shaded region in Fig. 5. As expected, the WDM case falls between the cold-matter and ideal-plasma limits.

These measurements of the mean ionization potential in a WDM plasma are a strong constraint on modeling of atomic physics and transport phenomena [58], as $\bar{I}$ can be straightforwardly calculated from any electronic structure model. Theoretical values of $\bar{I}$ are calculated in the cold ($\bar{I} = 54.7$ eV) and WDM ($\bar{I} = 45.7^{+3.1}_{-6.8}$ eV) cases using a Kohn-Sham density-functional theory and shown in Fig. 5. While this theory slightly underpredicts the data and Andersen-Ziegler values in the cold-matter case, it is in good agreement with the data in the WDM case. Additional tests of such electronic structure models or density functional theory predictions [59] are valuable as these models are applicable to a wide range of transport properties in

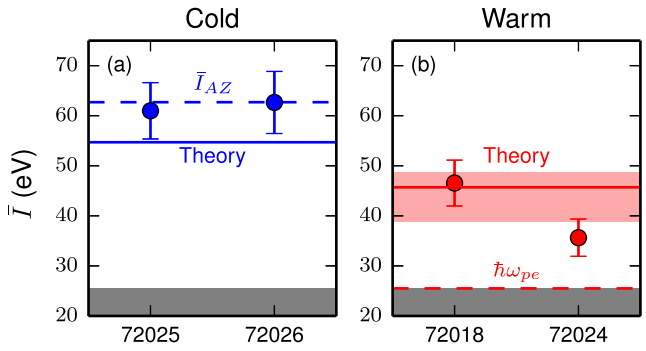

FIG. 5 (color online). Mean ionization potential ($\bar{I}$) inferred from the stopping-power data in the cold (a) and warm (b) cases compared to the Andersen-Ziegler empirical fits ($\bar{I}_{AZ}$), the ideal plasma case ($\hbar\omega_{pe}$), and electronic structure theory.

dense plasmas, for example, the phenomena of ionization potential depression [60,61], which is the subject of intensive recent study [62,63], is connected to the mean ionization potential as studied in this work. Other WDM collisional transport rates, such as resistivity and thermal conductivity, cannot be directly tested using this technique, but can be separately calculated using models like the AA-LDA in this work.

In conclusion, we report the first high-precision energy-loss measurements for energetic D^3He protons traversing an isochorically heated WDM Be plasma, which show an enhanced stopping power relative to cold matter. By using high-energy protons, the measurement is insensitive to temperature and degeneracy effects, and we thus probe the relative importance of the inhomogeneous electron distribution (bound states) on the stopping power. The partially-ionized material may be treated by an *ad hoc* combination of independent bound and free components, using the AA-LDA model, or by using a Bethe-style mean ionization potential. The first two models from previous theoretical work are found to be in good agreement with our experimental results. We also use the stopping data to infer $\bar{I}$ in this WDM plasma and compare to results from density functional theory, showing good agreement; this technique is an effective constraint on electronic structure models in WDM. In addition to the basic physics, accurate treatment of stopping in partially ionized material is particularly relevant to heavy-ion fusion, proton fast ignition, and hot-spot ignition with ablator materials mixed into the fuel.

Accurate theory of charged-particle stopping in dense, degenerate, strongly-coupled and/or partially-ionized plasmas is a fundamental challenge. We anticipate that this technique will be a robust platform for further stopping-power studies, such as probing at various electron degeneracies, plasma couplings, degrees of ionization, and with other materials to further constrain modeling of WDM plasma physics and stopping in partially ionized material. Finally, lower-energy particles such as DD-p, DD-T, and D^3He-α will be used to increase the experimental sensitivity to temperature and degeneracy effects.

We thank the operations crews and engineering staff at OMEGA for supporting these experiments, and E. Doeg and R. Frankel for their work processing the CR-39. This work was supported in part by the U.S. DOE (Grants No. DE-NA0001857, No. DE-FC52-08NA28752), LLNL (No. B597367), LLE (No. 415935- G), the Fusion Science Center at the University of Rochester (No. 524431), and the National Laser Users Facility (No. DE-NA0002035). This material is based upon work supported by the National Science Foundation Graduate Research Fellowship Program under Grant No. 1122374. The work of S. B. H. and P. E. G. was supported by the U.S. Department of Energy, Office of Science Early Career Research Program, Office of Fusion Energy Sciences.

*zylstra@mit.edu

[1] R. Zwanzig, *Nonequilibrium Statistical Mechanics* (Oxford University Press, New York, 2001).
[2] Z. Donkó and B. Nyíri, Phys. Plasmas **7**, 45 (2000).
[3] J. Daligault and G. Dimonte, Phys. Rev. E **79**, 056403 (2009).
[4] L. X. Benedict *et al.*, Phys. Rev. E **86**, 046406 (2012).
[5] S. Vinko, O. Ciricosta, and J. Wark, Nat. Commun. **5**, 3533 (2014).
[6] G. Gregori, S. H. Glenzer, W. Rozmus, R. W. Lee, and O. L. Landen, Phys. Rev. E **67**, 026412 (2003).
[7] S. J. Rose, J. Phys. B **25**, 1667 (1992).
[8] J. Nuckolls, L. Wood, A. Thiessen, and G. Zimmerman, Nature (London) **239**, 139 (1972).
[9] J. Lindl, Phys. Plasmas **2**, 3933 (1995).
[10] S. W. Haan *et al.*, Phys. Plasmas **2**, 2480 (1995).
[11] G. Miller, E. Moses, and C. Wuest, Nucl. Fusion **44**, S228 (2004).
[12] O. Hurricane *et al.*, Nature (London) **506**, 343 (2014).
[13] S. Humphries Jr., Nucl. Fusion **20**, 1549 (1980).
[14] M. Tabak, J. Hammer, M. E. Glinsky, W. L. Kruer, S. C. Wilks, J. Woodworth, E. M. Campbell, M. D. Perry, and R. J. Mason, Phys. Plasmas **1**, 1626 (1994).
[15] M. Roth *et al.*, Phys. Rev. Lett. **86**, 436 (2001).
[16] N. Bohr, Philos. Mag. **30**, 581 (1915).
[17] H. Bethe, Ann. Phys. (Berlin) **397**, 325 (1930).
[18] F. Bloch, Ann. Phys. (Berlin) **408**, 285 (1933).
[19] J. Ziegler, J. Biersack, and U. Littmark, *The Stopping and Range of Ions in Matter* (Pergamon, New York, 1985).
[20] B. Trubnikov, *Particle Interactions in a Fully Ionized Plasma* (Consultant's Bureau, New York, 1965).
[21] C. K. Li and R. D. Petrasso, Phys. Rev. Lett. **70**, 3059 (1993); **114**, 199901(E) (2015).
[22] P. E. Grabowski, M. P. Surh, D. F. Richards, F. R. Graziani, and M. S. Murillo, Phys. Rev. Lett. **111**, 215002 (2013).
[23] J. Lindhard, Mat. Fys. Medd. K. Dan. Vidensk. Selsk **28**, 1 (1954).
[24] J. Jackson, *Classical Electrodynamics* (Wiley, New York, 1975).
[25] G. Maynard and C. Deutsch, Phys. Rev. A **26**, 665 (1982).
[26] D. H. H. Hoffmann, K. Weyrich, H. Wahl, D. Gardés, R. Bimbot, and C. Fleurier, Phys. Rev. A **42**, 2313 (1990).
[27] J. Jacoby *et al.*, Phys. Rev. Lett. **74**, 1550 (1995).
[28] M. Roth, C. Stöckl, W. Süß, O. Iwase, D. O. Gericke, R. Bock, D. H. H. Hoffmann, M. Geissel, and W. Seelig, Europhys. Lett. **50**, 28 (2000).
[29] D. G. Hicks *et al.*, Phys. Plasmas **7**, 5106 (2000).
[30] A. Frank *et al.*, Phys. Rev. Lett. **110**, 115001 (2013).
[31] J. A. Frenje *et al.*, Measurements of Charged-Particle Stopping around the Bragg Peak in High-Energy-Density Plasmas, Phys. Rev. Lett. (2015).
[32] F. Graziani *et al.*, High Energy Density Phys. **8**, 105 (2012).
[33] T. Boehly *et al.*, Opt. Commun. **133**, 495 (1997).
[34] C. K. Li *et al.*, Rev. Sci. Instrum. **77**, 10E725 (2006).
[35] The Be used was of 99.8% atomic purity, purchased from Goodfellow, with measured mass density $1.77 \pm 0.01\,\mathrm{g/cm^3}$. Each target plug was laser-machined from a single sheet with average thickness 532.1 μm and 1σ variation of 1.2 μm, so that each target had the same total ρL to within 0.2%.

[36] S. H. Glenzer, G. Gregori, F. J. Rogers, D. H. Froula, S. W. Pollaine, R. S. Wallace, and O. L. Landen, Phys. Plasmas **10**, 2433 (2003).
[37] N. Sinenian, M. J.-E. Manuel, J. A. Frenje, F. H. Séguin, C. K. Li, and R. D. Petrasso, Plasma Phys. Controlled Fusion **55**, 045001 (2013).
[38] The absence of electrical charging of the target, or electromagnetic deflections of protons was verified with proton radiography.
[39] S. H. Glenzer, G. Gregori, R. W. Lee, F. J. Rogers, S. W. Pollaine, and O. L. Landen, Phys. Rev. Lett. **90**, 175002 (2003).
[40] S. H. Glenzer, O. L. Landen, P. Neumayer, R. W. Lee, K. Widmann, S. W. Pollaine, R. J. Wallace, G. Gregori, A. Höll, T. Bornath, R. Thiele, V. Schwarz, W.-D. Kraeft, and R. Redmer, Phys. Rev. Lett. **98**, 065002 (2007).
[41] S. H. Glenzer and R. Redmer, Rev. Mod. Phys. **81**, 1625 (2009).
[42] X-ray Thomson scattering to diagnose the Be-plasma conditions simultaneously with the stopping-power measurement was unsuccessful, so we use results previously reported for the determination of T_e and n_e.
[43] F. Séguin *et al.*, Rev. Sci. Instrum. **74**, 975 (2003).
[44] F. H. Séguin, N. Sinenian, M. Rosenberg, A. Zylstra, M. J.-E. Manuel, H. Sio, C. Waugh, H. G. Rinderknecht, M. G. Johnson, J. Frenje, C. K. Li, R. Petrasso, T. C. Sangster, and S. Roberts, Rev. Sci. Instrum. **83**, 10D908 (2012).
[45] The spectrometers employ a single-particle-counting technique using CR-39, with resulting signal-to-noise ratio ~100. The ~40 keV energy uncertainty is dominated by the CR-39 proton response (see Ref. [44]).
[46] N. Sinenian *et al.*, Rev. Sci. Instrum. **83**, 043502 (2012).
[47] For these conditions the path- and linear-distance energy losses are equivalent to better than 0.1%, since large-angle Coulomb scattering is negligible.
[48] International Commission on Radiation Units and Measurements, ICRU Report 49, Stopping Powers and Ranges for Protons and Alpha Particles (1993).
[49] T. A. Mehlhorn, J. Appl. Phys. **52**, 6522 (1981).
[50] G. Zimmerman, LLNL, Report No. UCRL-JC-105616 (1990).
[51] I. Nagy and B. Apagyi, Phys. Rev. A **58**, R1653 (1998).
[52] G. Faussurier, C. Blancard, P. Cossé, and P. Renaudin, Phys. Plasmas **17**, 052707 (2010).
[53] L. S. Brown, D. L. Preston, and R. L. Singleton Jr., Phys. Rep. **410**, 237 (2005).
[54] S. B. Hansen, A. Y. Faenov, T. A. Pikuz, K. B. Fournier, R. Shepherd, H. Chen, K. Widmann, S. C. Wilks, Y. Ping, H. K. Chung, A. Niles, J. R. Hunter, G. Dyer, and T. Ditmire, Phys. Rev. E **72**, 036408 (2005).
[55] D. Gericke, M. Schlanges, and W. Kraeft, Phys. Lett. A **222**, 241 (1996).
[56] G. Röpke, R. Redmer, A. Wierling, and H. Reinholz, Phys. Plasmas **7**, 39 (2000).
[57] H. Andersen and J. Ziegler, *Hydrogen Stopping Powers and Ranges in All Elements* (Pergamon, New York, 1979).
[58] D. Ballester and I. M. Tkachenko, Phys. Rev. Lett. **101**, 075002 (2008).
[59] M. S. Murillo, J. Weisheit, S. B. Hansen, and M. W. C. Dharma-wardana, Phys. Rev. E **87**, 063113 (2013).
[60] G. Ecker and W. Kröll, Phys. Fluids **6**, 62 (1963).
[61] J. C. Stewart and K. D. Pyatt, Jr., Astrophys. J. **144**, 1203 (1966).
[62] O. Ciricosta *et al.*, Phys. Rev. Lett. **109**, 065002 (2012).
[63] D. J. Hoarty, P. Allan, S. F. James, C. R. D. Brown, L. M. R. Hobbs, M. P. Hill, J. W. O. Harris, J. Morton, M. G. Brookes, R. Shepherd, J. Dunn, H. Chen, E. Von Marley, P. Beiersdorfer, H. K. Chung, R. W. Lee, G. Brown, and J. Emig, Phys. Rev. Lett. **110**, 265003 (2013).